Understanding Pulsar Radio Emission

R. T. Gangadhara
Indian Institute of Astrophysics, Bangalore, India

Collaboration: JinLin Han and group, NAOC

FPS-Special: Magnetospheric Dynamics, 11-13 October 2019

Outline

- Introduction
- Viewing Geometry of Pulsar Radio Emission
- Mechanism of Radio Emission?
  - Incoherent Radiation
  - Coherent Radiation:
- Perturbations:
  - Rotation
  - Polar Cap Current
- Conclusion

Detection: Jocelyn Bell and Tony Hewish (1967)
Proposed: Rapidly Spinning Neutron Starts.

Pulse intensity fluctuations

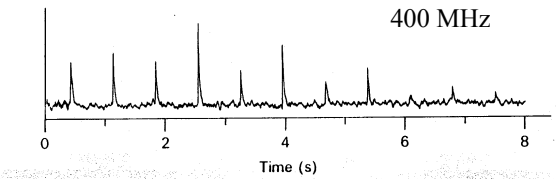

Individual pulses from PSR B0329+54

Manchester & Taylor (1977)

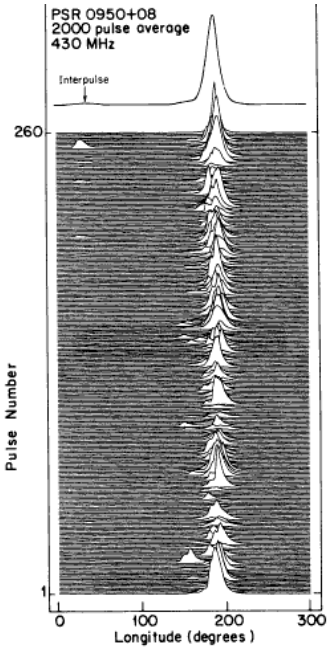

PSR B0950+08
Pulse-to-pulse fluctuations

Hankins & Cordes (1981)

Hollow Cone Model

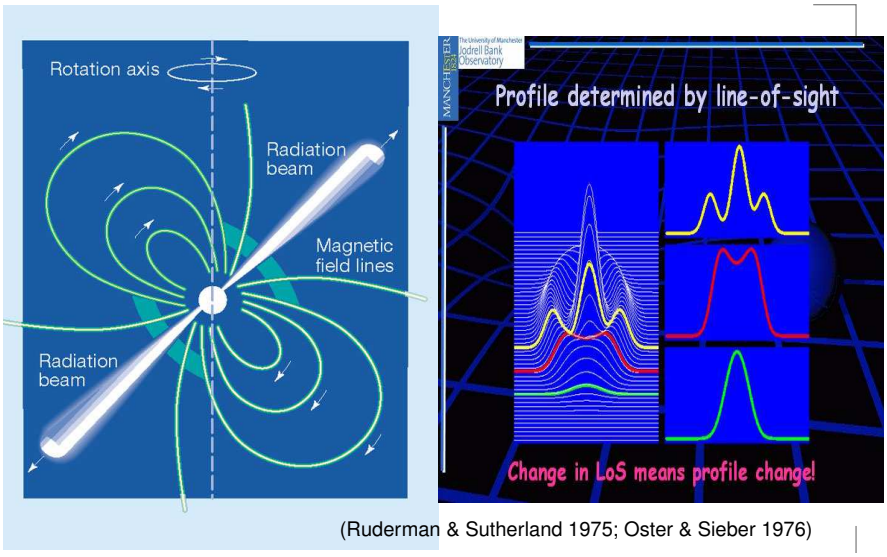

(Ruderman & Sutherland 1975; Oster & Sieber 1976)

Average pulsar profiles

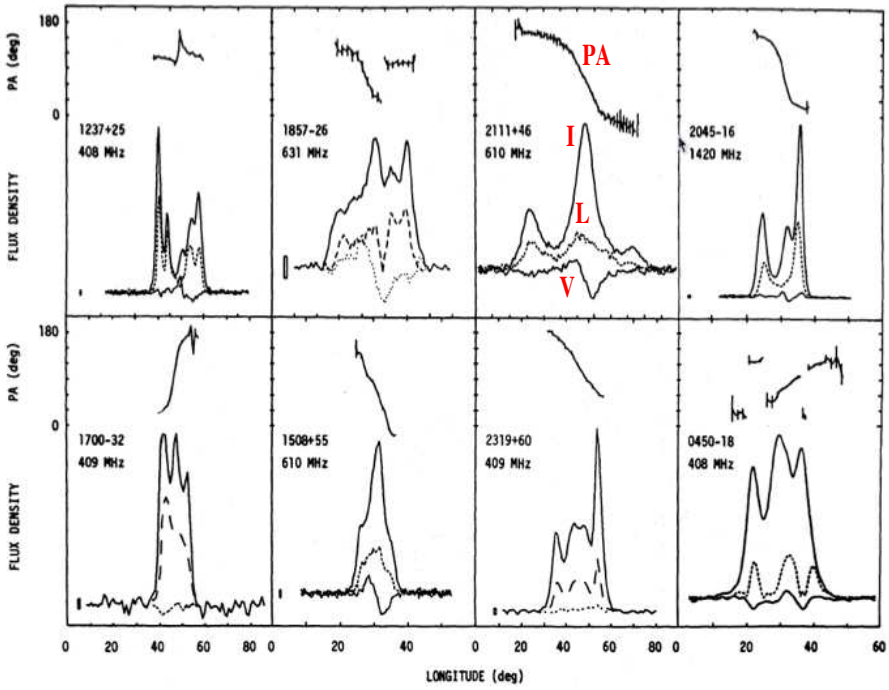

Gould (1994)

Viewing Geometry of Pulsar Radio Emission

The visibility of pulsar radio emission is a geometric problem: Identify the "visible point" in the pulsar magnetosphere that an observer can see.

- Assumptions:
  - Magnetic field is dipolar
  - Emission occurs only within the open-field region (polar cap)
  - Emission is confined to a narrow beam around the direction of tangent to the magnetic field line (e.g., Jackson 1975)
- Two angles are deduced for a given pulsar:

  - Obliquity angle, α, between the magnetic axis and the rotation axis
  - Viewing angle, ζ , between the line of sight and the rotation axis.

  Then the line of sight impact parameter $\beta = \zeta - \alpha$.

The Tangent Model

- (r, θ, ϕ), relative to the magnetic axis (rotating frame), or
- (r, Θ, Φ), relative to the rotation axis (observer frame).

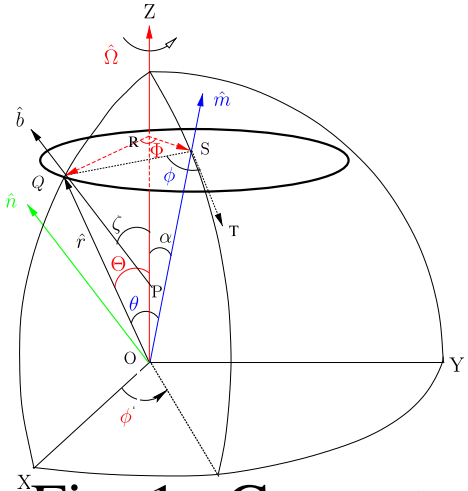

Fig. 1. Geometry

Rotation phase $\phi' = \Omega t$. The emission height r is determined: A/R effects (e.g., Gangadhara and Gupta 2001; Gupta and Gangadhara 2003; Gangadhara 2004, 2005).

Tangent Model : $\hat{n} \cdot \hat{b} = 1$

Eq. for field line: $r = r_e \sin^2\theta$ (Alfvén & Falthammar 1963)

Position vectors: $r_{\text{mag}} = r\{\sin\theta\cos\phi,\ \sin\theta\sin\phi,\ \cos\theta\}$

$r_{\text{lab}} = r\{\sin\Theta\cos\Phi,\ \sin\Theta\sin\Phi,\ \cos\Theta\}$

Transformation: $r_{\text{lab}} = \Lambda \,.\, r_{\text{mag}}$, where $\Lambda = \begin{pmatrix} \cos\alpha\cos\phi' & -\sin\phi' & \cos\phi'\sin\alpha \\ \cos\alpha\sin\phi' & \cos\phi' & \sin\alpha\sin\phi' \\ -\sin\alpha & 0 & \cos\alpha \end{pmatrix}$

Opening angle of the emission beam:

$$\Gamma = \cos^{-1}(\cos\alpha\cos\zeta + \sin\alpha\sin\zeta\cos\phi')$$

$$\theta = \frac{1}{2}\cos^{-1}\left[\frac{1}{3}\left(\cos\Gamma\sqrt{8+\cos^2\Gamma} - \sin^2\Gamma\right)\right]$$

$$\phi = \tan^{-1}\left(\frac{\sin\phi'\sin\zeta}{\sin\alpha\cos\zeta - \cos\alpha\sin\zeta\cos\phi'}\right)$$

Rotation axis centered co-ordinates:

$$\Theta = \cos^{-1}(\cos\alpha\cos\theta - \sin\alpha\sin\theta\cos\phi)$$

$$\Phi = \tan^{-1}\left((\sin\alpha\cot\theta\csc\phi\sin\phi' + \cos\alpha\cot\phi\sin\phi' + \cos\phi') / (\sin\alpha\cot\theta\csc\phi\cos\phi' + \cos\alpha\cot\phi\cos\phi' - \sin\phi')\right)$$

Spinning dipole

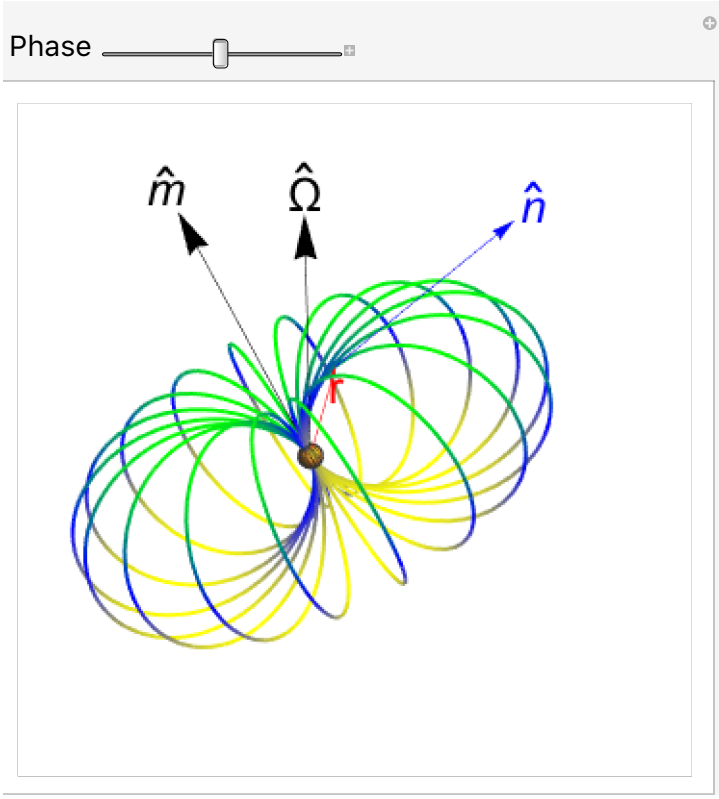

$$\hat{n} \cdot \hat{b} = 1$$

Emission Point Trajectory

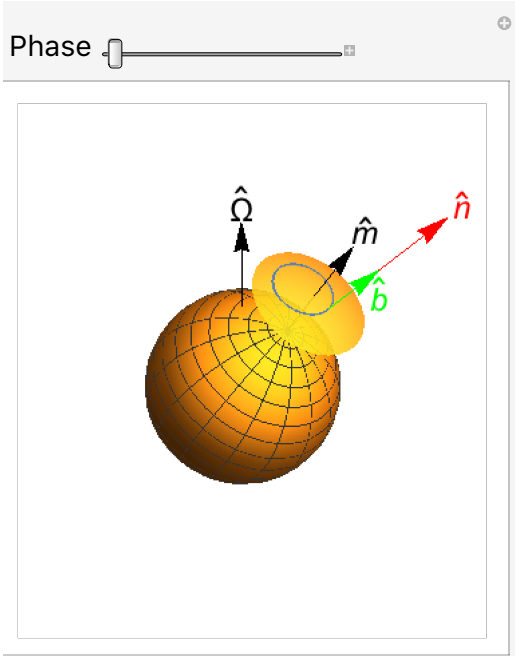

Note that there is a recent claim that this motion is observable using interstellar holography by Pen et al. (2014), and Yuen & Melrose (2014).

The **FAST** can be combined with other telescopes to form a very long baseline interferometer (VLBI) network, which can be used to accurately **locate emission regions of pulsar**.

Monthly Notices
of the
ROYAL ASTRONOMICAL SOCIETY

MNRASL **440,** L36–L40 (2014) doi:10.1093/mnrasl/slu010
Advance Access publication 2014 February 14

50 picoarcsec astrometry of pulsar emission

Ue-Li Pen,[1,2★] Jean-Pierre Macquart,[3,2★] Adam T. Deller[4★] and Walter Brisken[5,6★]

[1]*Canadian Institute for Theoretical Astrophysics, University of Toronto, ON M5S 3H8, Canada*
[2]*ARC Centre of Excellence for All-Sky Astrophysics (CAASTRO)*
[3]*ICRAR/Curtin University GPO Box U1987, Perth, WA 6845, Australia*
[4]*The Netherlands Institute for Radio Astronomy (ASTRON), PO Box 2, NL-7990 AA Dwingeloo, The Netherlands*
[5]*National Radio Astronomy Observatory, PO Box 0, Socorro, NM 87801, USA*
[6]*University of Minnesota*

Accepted 2014 January 14. Received 2014 January 9; in original form 2013 January 27

ABSTRACT

We use very long baseline interferometry (VLBI) imaging of the interstellar scattering speckle pattern associated with the pulsar PSR 0834+06 to measure the astrometric motion of its emission. The $D \sim 5$ au interstellar baselines, provided by interference between speckles spanning the scattering disc, enable us to detect motions with subnanoarcsecond accuracy. We measure a small pulse deflection of $\sim 18 \pm 2$ km (not including geometric uncertainties), which is 100 times smaller than the characteristic resolution (λ/D) of this interstellar interferometer. This implies that the emission region is small, and at an altitude of a few hundred km, with the exact value depending on field geometry. This is substantially closer to the star than to the light cylinder. Future VLBI measurements can improve on this finding. This new regime of ultraprecise astrometry may enable precision parallax distance determination of pulsar binary displacements.

Key words: techniques: high angular resolution – pulsars: individual: B0834+06 – ISM: structure astrometry.

We consider some limits that are exactly calculable. For simplicity, we assume the radiation to emit from the rotational equator, and our line of sight to be perpendicular to the spin axis. One case is that the emission region is very small, and the pulse period is determined by the beaming angle of the emission. In this case, the deflection of the pulse is just the height times the duty cycle, corresponding to an emission height of about 200 km.

Possibly the extreme antithetical model is one in which the emission is infinitely beamed radiating tangentially to the local magnetic field line. In this case, the altitude is related to the deflection by the field curvature. If we take the curvature to be roughly the altitude, as expected for a dipolar field, we obtain the same rough altitude as above. We note that this can be arbitrarily incorrect: in the unlikely extreme case that the field lines are purely radial with no curvature, there is no apparent motion, and the emission altitude could be arbitrarily high. In the infinite curvature limit, the emission is given by the same altitude as the beamed case.

From these scenarios we also see that the emission region generically has a smaller angular size than the displacement during the pulse: in the infinitely beamed scenario we only see the one field line tangential to our line of sight, resulting in an infinitesimal apparent emission size. In the first scenario, we see all field lines which are within one beaming angle of our line of sight. The size of the emission region plus the beaming angle must be less than the pulse duration, while the deflection is given by the beaming angle. There could be exotic counter examples, for example if the field lines were convergent at the emission region.

A dual representation could have been done in terms of a correlation function. We refer the interested reader to the cosmological literature (e.g. Pen, Van Waerbeke & Mellier 2002, and references therein).

Mechanism of Radio Emission?

- Pulsar radio emission is coherent and highly polarized (e.g., Lyne & Manchester 1988; Rankin 1990, 1993).

- Rotating magnetic field induces a strong electric field which accelerates relativistic charged particles (primary), which emit γ-rays. Next, γ-rays create secondary pair (e^+, e^-) – plasma, which in turn corotates with the magnetosphere (Ruderman & Sutherland 1975).

- Radio emission models assume (1) radiation is emitted by the relativistic plasma in the direction of field line tangents, and (2) polarized in the plane of dipolar field lines.

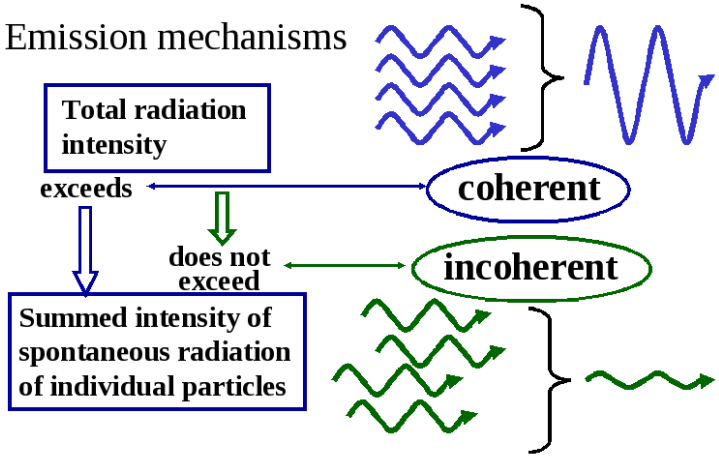

Mechanism of Radio Emission

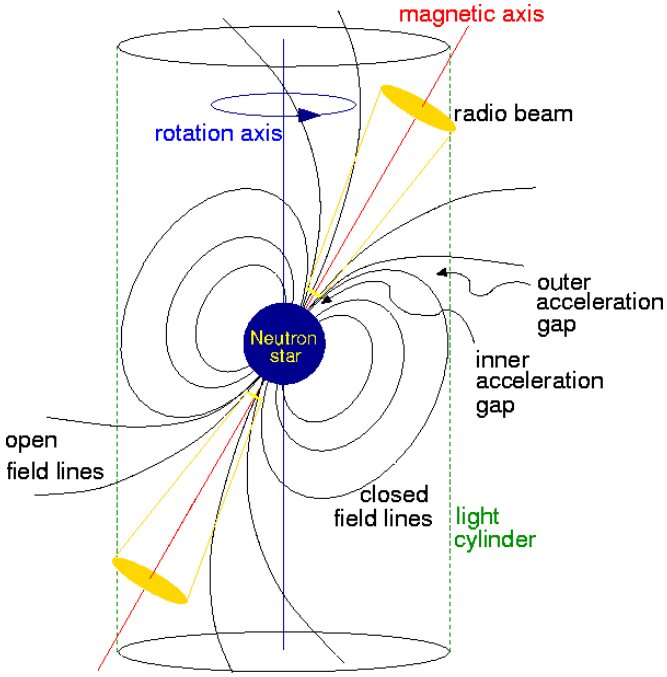

Incoherent Emission Mechanisms

- Single particle curvature radiation

  (*e.g.,* Sturrock 1971; Ruderman & Sutherland 1975; Gangadhara 2010; Wang, Wang & Han 2012)

- Cyclotron/Synchrotron radiation (*e.g.,* Rybicki & Lightman 1979)
- Thermal radiation: Black body
- Inverse Compton Scattering (ICS)

  (*e.g.,* Zhang, Hong, and Qiao 1999; Lv et al. 2011)

Pulsar Radio Emission

Curvature Radiation

Relatvistic charged particles (e^+, e^-) moving along the curved magnetic field lines experience curvature acceleration, and hence radiate the electromagnetic waves.

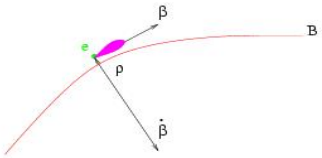

The frequency of radiation:

$$\nu_c = \frac{3}{4\pi}\gamma^3\frac{c}{\rho}$$

The power radiated by particles:

$$P = \frac{2}{3}\frac{q^2}{c}\gamma^4\left(\frac{c}{\rho}\right)^2$$

ρ = Radius of curvature of filed lines,
$\gamma = 1/\sqrt{1-\beta^2}$ Lorentz factor.

Electric field of curvature radiation

Relativistic bunch emits radiation as it accelerates along the curved trajectory. The radiation field at observer (Jackson 1975):

$$\boldsymbol{E}(\boldsymbol{r},t) = \frac{q}{c}\left[\frac{\hat{n}\times[(\hat{n}-\boldsymbol{\beta})\times\dot{\boldsymbol{\beta}}]}{R\,\xi^3}\right]_{\rm ret},$$

$\xi = 1-\boldsymbol{\beta}\cdot\hat{n}$ the beaming factor,
$\boldsymbol{\beta} = \boldsymbol{v}/c$ the velocity,
$\dot{\boldsymbol{\beta}} = \boldsymbol{a}/c$ the acceleration ,
R is the distance from radiating region to observer,
$\hat{n} = (\sin\zeta,\ 0,\ \cos\zeta)$ the sight line, and
$\zeta = \alpha+\sigma$ the angle between $\hat{n}$ and $\hat{\Omega}$.

$$\begin{aligned} E_{\parallel} &= \hat{\epsilon}_{\parallel}\cdot\boldsymbol{E} = -\cos\zeta\,E_{\rm x}+\sin\zeta\,E_{\rm z}\ , \\ E_{\perp} &= \hat{\epsilon}_{\perp}\cdot\boldsymbol{E} = E_{\rm y}\ . \end{aligned}$$

Five component pulse

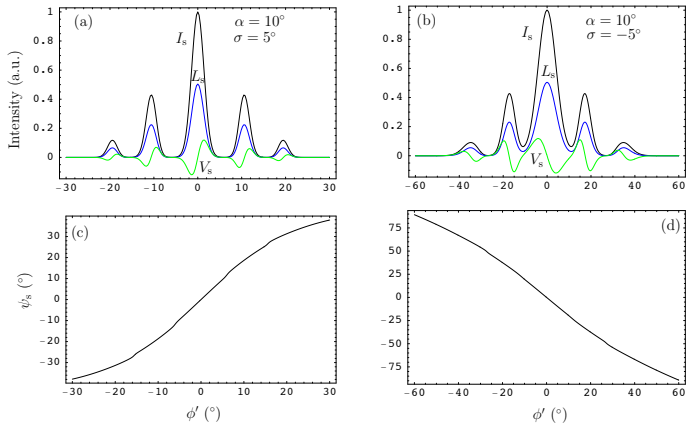

Fig. 7. Simulated pulse profiles. For panels (a) and (c) used $\sigma_\theta = \sigma_\phi = 0.14,\ 0.10,\ 0.07,$ $\theta_p = 3.33^\circ,\ 3.66^\circ,\ 4.32^\circ, \phi_p = 0^\circ,\ \pm 30^\circ,\ \pm 50^\circ,$ and $f_0 = 1,\ 0.75,\ 0.5,$ respectively, for the Gaussians. Similarly, for panels (b) and (d) used $\sigma_\theta = \sigma_\phi = 0.14,\ 0.06,\ 0.03,$ $\theta_p = 3.33^\circ,\ 3.62^\circ,\ 4.38^\circ, \phi_p = 180^\circ,\ 180^\circ \pm 16^\circ,\ 180^\circ \pm 26^\circ,$ and $f_0 = 1,\ 0.75,\ 0.5.$

$\Omega = 0,$ J=0

Coherent Emission Mechanisms

- **Antenna Mechanisms - emission by bunches**
  (e.g., Sturrock 1971; Ruderman & Sutherland 1975; Benford & Buschauer 1977; Melrose 1981, 1992, 1993)

- **Plasma Instabilities - relativistic plasma wave emission**
  (e.g., Melrose & Stoneham 1977; Melrose 1979; Volokitin, Krasnoselskikh & Machabeli 1985; Arons & Barnard 1986; Beskin, Gurevich & Istomin 1986, 1988, 1993; Lominadze et al. 1986; Kazbegi, Machabeli & Melikidze 1991; Asseo 1993; Luo, Machabeli & Melrose 1994)

- **Maser Mechanisms - maser curvature emission**
  (e.g., Zheleznyakov & Shaposhnikov 1979; Chugunov & Shaposhnikov 1988; Luo & Melrose 1992; Luo & Melrose 1994)

The physical mechanism of pulsar radio emission remains still poorly understood.

Radio emission due to plasma bunch

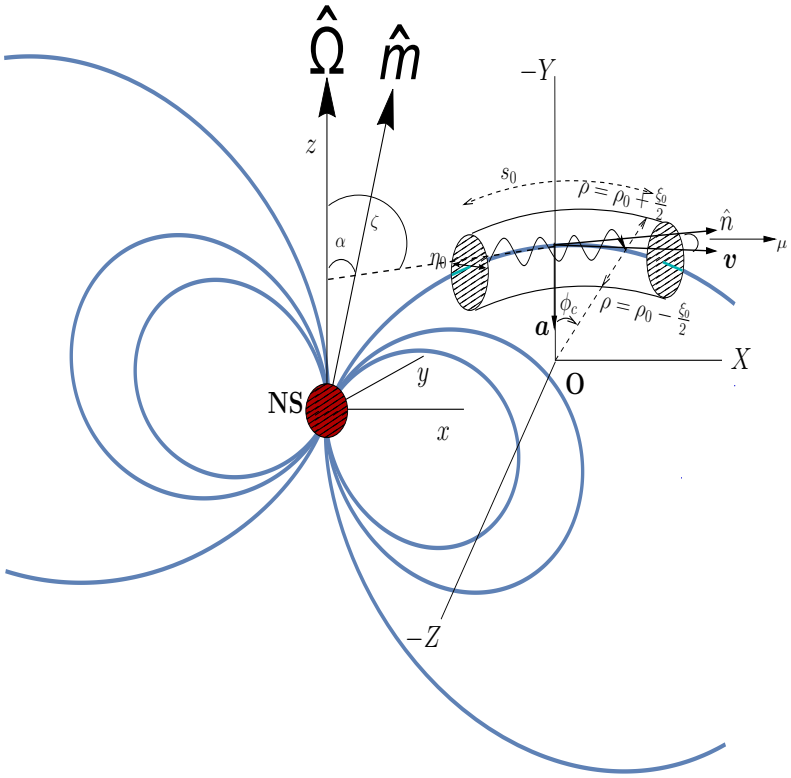

Figure 9. Geometry for collective plasma radio emission from a cylindrical bunch in pulsar magnetosphere. The Cartesian coordinate system-xyz is the observer frame whose origin is at the center of NS. $\hat{\boldsymbol{m}}$ is the magnetic axis which is inclined by an angle α with respect to spin axis $\hat{\boldsymbol{\Omega}}$. The line of sight of observer is $\hat{\boldsymbol{n}}$. The bunch dimensions (s_0, ρ_0, η_0) are the length, radius and height, respectively. ξ_0 is the radial width of bunch, and ϕ_c is the angle subtended by the position vector of an arbitrary point in the bunch with respect to Y-axis. $\boldsymbol{v}$ and $\boldsymbol{a}$ are the center of momentum (CM) velocity and acceleration of the bunch. The Cartesian coordinate system-XYZ is chosen in such way that X-axis is parallel to the line of sight $\hat{\boldsymbol{n}}$, $-Y$-axis is parallel to the curvature vector $\hat{\boldsymbol{k}}_{\rm t}$ and $-Z$-axis parallel to the bi-normal $\hat{\boldsymbol{b}}_{\rm nt}$. *Tridib and Gangadhara (2019)*

The relativistic plasma bunches can support the growth and decay of plasma waves. They can coherently radiate the radio waves due to curvature acceleration.

$R_0 = 4\ \text{kpc},\ \alpha = 30^\circ,\ \sigma = 2^\circ,\ P = 1\ \text{s},\ \gamma = 500,\ n = 10^{12}\ \text{cm}^{-3}$

Coherent emission

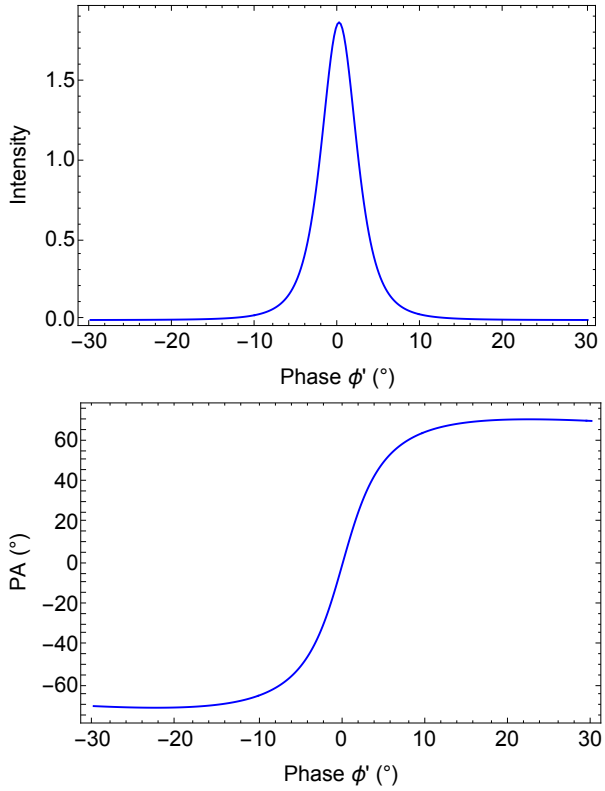

Incoherent emission

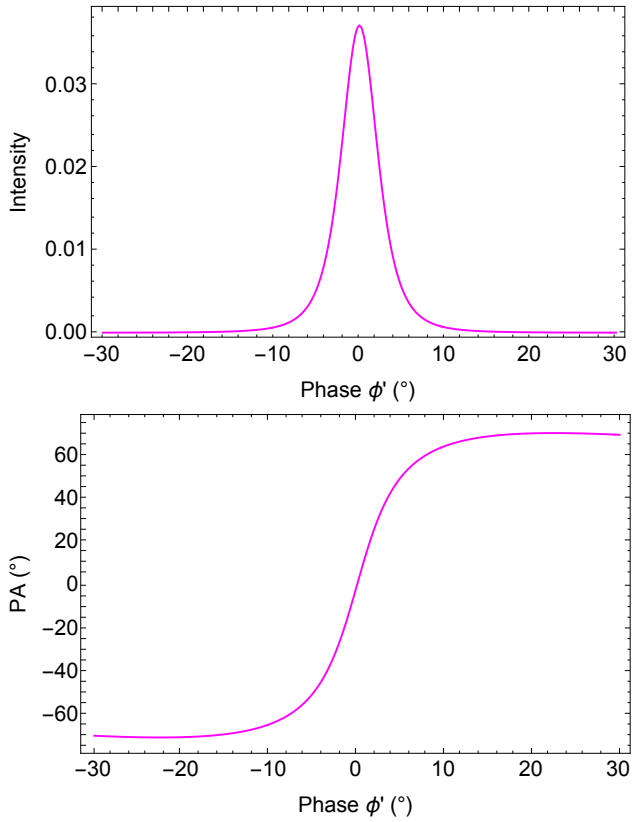

The difference coherent and incoherent emission

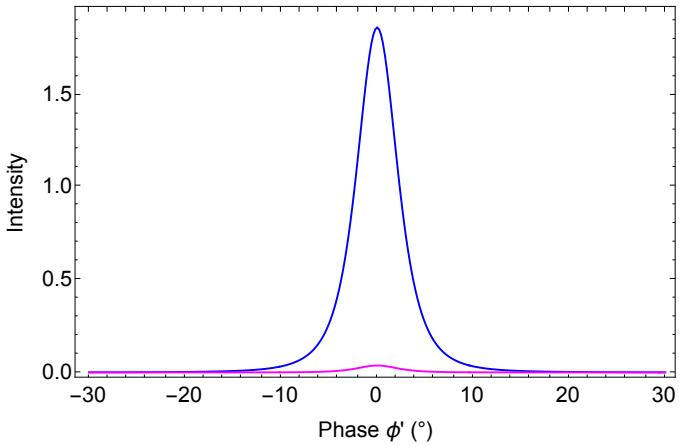

Brightness temperature (Cordes 1979):

$$T_{\mathrm{b}} = \frac{1}{2k_{\mathrm{B}}} \frac{\lambda^2 S_\nu}{(c\Delta t/R)^2},$$

where $S_\nu = \frac{c}{T} I_\nu$.

Perturbations

Aberration of pulsar radiation

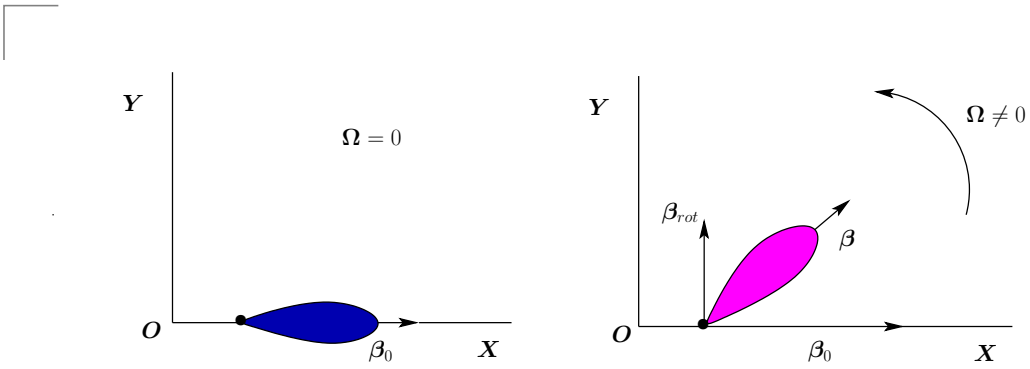

Velocity of bunch: $\boldsymbol{\beta}_0 = \boldsymbol{v}_0/c$

Rotation velocity of bunch: $\boldsymbol{\beta}_{\rm rot} = \boldsymbol{\Omega} \times \boldsymbol{r}/c$

(Gangadhara 2005; Kumar and Gangadhara 2012; Wang , Wang and Han 2012)

Retardation of pulsar radiation

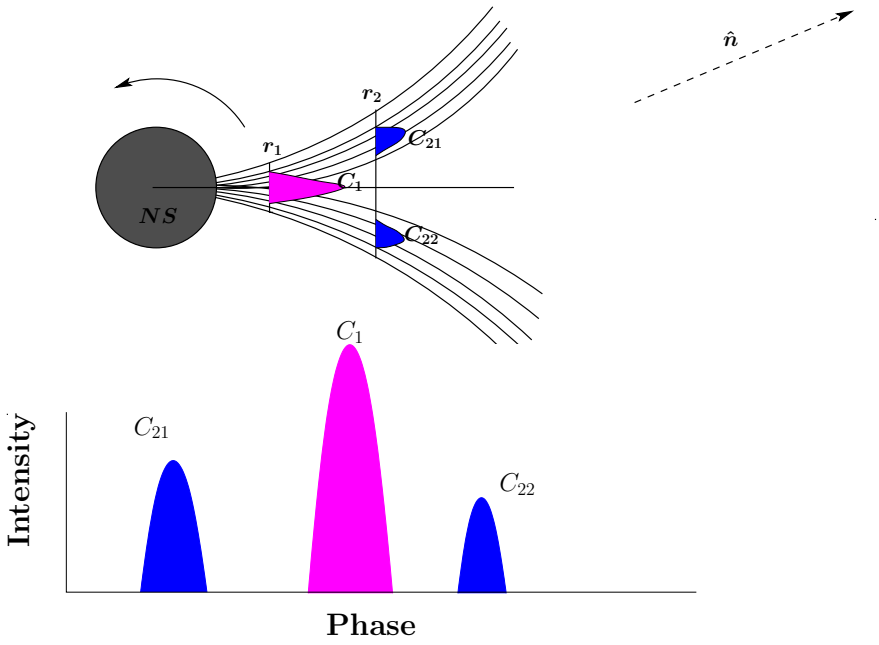

(Gangadhara 2005)

PC–Current perturbation of Magnetic Field

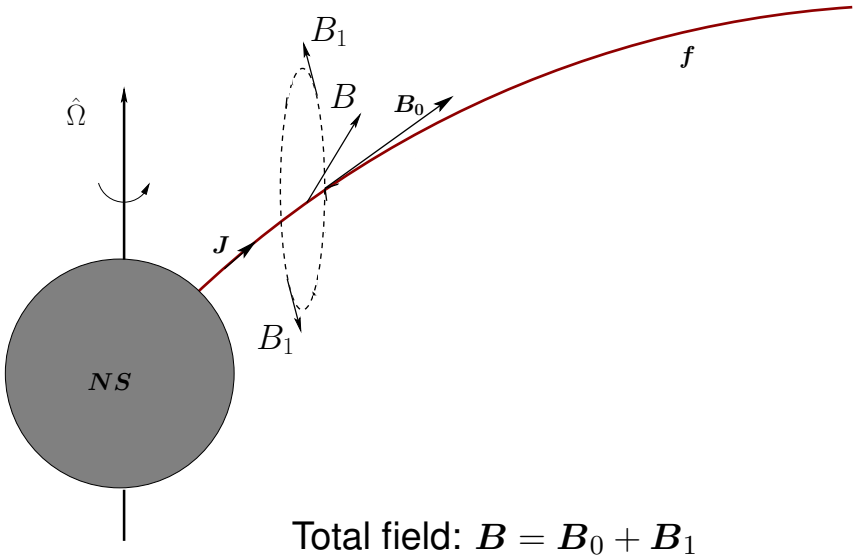

Total field: $\boldsymbol{B} = \boldsymbol{B}_0 + \boldsymbol{B}_1$

(Gangadhara 2005; Kumar and Gangadhara 2012b)

Effect of rotation and polar cap current

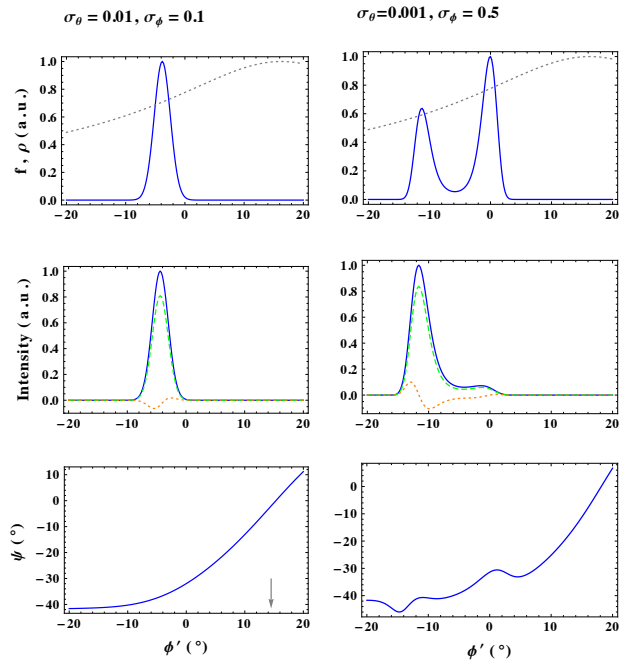

Figure 8: Simulated pulse profiles with the nonuniform distribution of sources in both the polar and azimuthal directions, after considering the perturbations by the rotation and PC–current with $\sigma_\theta = 5^\circ$, r_n=0.1, f_0=1, $\theta_p = 3.4^\circ$, $\varphi_p = 0^\circ$. *Dinesh and Gangadhara (2013).*

Conclusion

- Pulsar radio emission is due to relativistic pair plasma accelerated along dipolar magnetic field lines.
- The coherent curvature radiation can explain most of the polarization characteristics of radio pulsars.
- By incorporating coherent mechanism in curvature emission we can explain the high brightness temperature of radio pulsars $\sim 10^{25}$ K

Thank you